Supplementary Material

S1. MODEL CALCULATIONS OF THE LOCAL DENSITY OF STATES (LDOS)

The differential tunneling current imaged in STM is proportional to LDOS(eV, $\mathbf{r}$), where eV is the bias voltage, and the local density of states (LDOS) is given by

$$\mathrm{LDOS}(E,\mathbf{r}) = -\tfrac{1}{\pi}\mathrm{Im}\langle c_{\mathbf{r}} c^{\dagger}_{\mathbf{r}}\rangle_E = -\tfrac{1}{\pi}\mathrm{Im}G(E,\mathbf{r}) \tag{S1}$$

where $c^{\dagger}_{\mathbf{r}}$ is the electron creation operator and $G(E,\mathbf{r})$ is the electron Green's function. To relate the continuum electronic density of states to the wavefunctions of a lattice model, we expand the continuum electron operator in terms of lattice creation operators associated to an orbital α and a lattice site $\mathbf{R}$, via $c^{\dagger}_{\mathbf{r}} = \sum_{\alpha\mathbf{R}} w_{\alpha\mathbf{R}}(\mathbf{r}) c^{\dagger}_{\alpha\mathbf{R}}$ where $w_{\alpha\mathbf{R}}(\mathbf{r})$ are a set of real space orbitals indexed by α and centered at the lattice sites $\mathbf{R}$, e.g. [53, 54]. One obtains

$$\begin{aligned}\mathrm{LDOS}(E,\mathbf{r}) &= -\tfrac{1}{\pi}\mathrm{Im}\sum_{\alpha\alpha',\mathbf{R}\mathbf{R}'} w^{*}_{\alpha\mathbf{R}}(\mathbf{r}) w_{\alpha'\mathbf{R}'}(\mathbf{r})\langle c_{\alpha\mathbf{R}} c^{\dagger}_{\alpha'\mathbf{R}'}\rangle_E \\ &= -\tfrac{1}{\pi}\mathrm{Im}\sum_{\alpha\alpha',\mathbf{R}\mathbf{R}'} w^{*}_{\alpha\mathbf{R}}(\mathbf{r}) w_{\alpha'\mathbf{R}'}(\mathbf{r}) G(E,\mathbf{R}-\mathbf{R}')_{\alpha\alpha'}\end{aligned} \tag{S2}$$

where $G(E,\mathbf{R}-\mathbf{R}')_{\alpha\alpha'}$ is the Green's function of the lattice model,

$$G(E,\mathbf{R}-\mathbf{R}')_{\alpha\alpha'} = \int \frac{d^d\mathbf{k}}{(2\pi)^d}\left(\frac{1}{E-\mathcal{H}(\mathbf{k})+i0}\right)_{\alpha\alpha'} e^{i\mathbf{k}(\mathbf{R}-\mathbf{R}')} \tag{S3}$$

where $\mathcal{H}(\mathbf{k})_{\alpha\alpha'}$ is the tight-binding Hamiltonian, defined as a matrix acting on the basis of orbitals α.

A. Charge density in three-band model of WSe_2

In this section, we present calculations of the local density of states (LDOS) in a widely-used minimal three-band model of WSe_2 [23], comprised of d_{z^2}, d_{xy}, and $d_{x^2-y^2}$ orbitals located on the triangular lattice formed by the tungsten atoms. The model is given by

$$H^{\mathrm{NN}}(\boldsymbol{k}) = \begin{bmatrix} h_0 & h_1 & h_2 \\ h_1^* & h_{11} & h_{12} \\ h_2^* & h_{12}^* & h_{22}\end{bmatrix} \tag{S4}$$

where

$$h_0 = 2t_0(\cos 2\alpha + 2\cos\alpha\cos\beta) + \epsilon_1, \tag{S5}$$

$$h_1 = -2\sqrt{3}t_2\sin\alpha\sin\beta + 2it_1(\sin 2\alpha + \sin\alpha\cos\beta), \tag{S6}$$

$$h_2 = 2t_2(\cos 2\alpha - \cos\alpha\cos\beta) + 2\sqrt{3}it_1\cos\alpha\sin\beta, \tag{S7}$$

$$h_{11} = 2t_{11}\cos 2\alpha + (t_{11}+3t_{22})\cos\alpha\cos\beta + \epsilon_2, \tag{S8}$$

$$h_{22} = 2t_{22}\cos 2\alpha + (3t_{11}+t_{22})\cos\alpha\cos\beta + \epsilon_2 \tag{S9}$$

$$h_{12} = \sqrt{3}\,(t_{22}-t_{11})\sin\alpha\sin\beta + 4it_{12}\sin\alpha(\cos\alpha-\cos\beta) \tag{S10}$$

$$(\alpha,\beta) = (k_x a/2, \sqrt{3}k_y a/2) \tag{S11}$$

with the hopping values for WSe_2 given by $t_0 = -0.146$, $t_1 = -0.124$, $t_2 = 0.507$, $t_{11} = 0.117$, $t_{12} = 0.127$, $t_{22} = 0.015$, $\epsilon_1 = 0.728$, $\epsilon_2 = 1.655$ (all units in eV). We retained only nearest-neighbour hoppings; we shall present calculations with spin-orbit set to zero, to highlight that it is irrelevant to the essential physics of the C_3-enforced obstruction.

The tight-binding Hamiltonian accurately captures the mismatch of C_3 eigenvalues in the valence band – the valence band wavefunction has a C_3 eigenvalue of 1 near Γ and $\omega = e^{2\pi i/3}$ near K. The difference in C_3 eigenvalues implies that the valence band is described by an obstructed atomic limit, meaning that it is not possible to construct a real-space basis for this band out of states exponentially localised on the atomic sites, using only the Bloch states from this band. Calculating the LDOS in this minimal model serves to illustrate that this key feature is the origin of the charge shifting, rather than any additional details captured in full DFT calculations of the charge density.

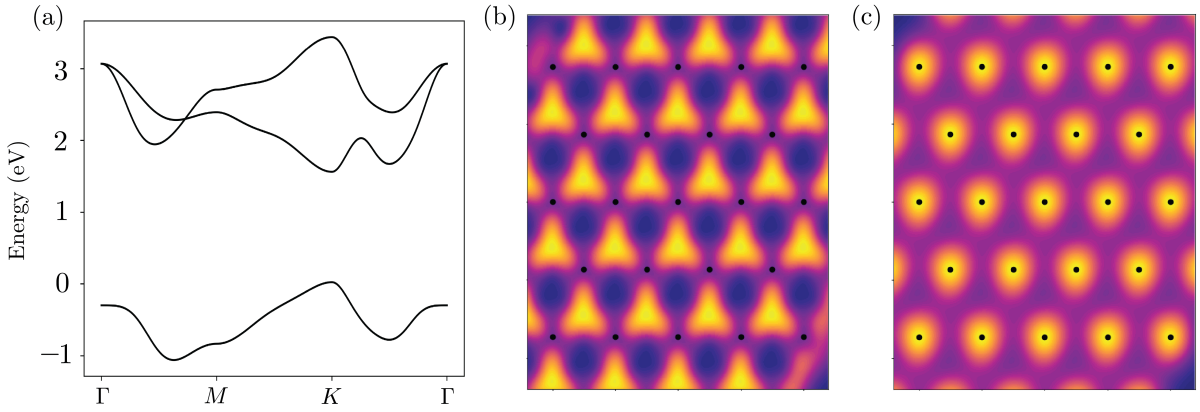

FIG. S1. **Simulated local density of states in the three-band model of WSe_2.** (a) Band structure of WSe_2 in the minimal three-band model of Ref. [23], Eq. (S4). Note the neglect of spin-orbit coupling results in minor qualitative differences from Fig. 3c. (b) The local density of states in the three-band model near $E = 0$, where the Fermi surface is close to the K-point, illustrating the localisation of charge in the center of the triangles (dark spots indicate the locations of the W atoms). (c) Local density of states near $E = -0.3$, where a sizable pocket near Γ contributes, producing atomically-centered charge density.

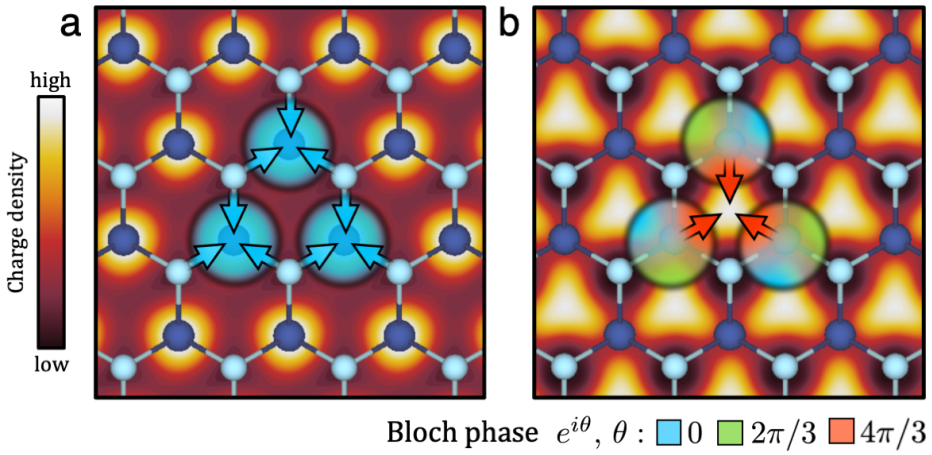

FIG. S2. **Off-centered charge density from orbital interference.** In addition to the Wannier function viewpoint described in the main text Fig. 2, the off-centered charge density can be understood in terms of the overlap between the valence band and constituent atomic orbitals. (a) Near Γ, the orbital weight has trivial C_3 eigenvalue, and the charge density has the same phase everywhere near the atomic sites. (b) Near K, the valence band has $d + id$ character – at each atomic site, the orbitals exhibit a phase winding indicated by the red/green/orange pinwheel; these phases add constructively near the hollow sites.

In Fig. S1a, we show the resulting band structure with orbital weight overlaid. In this minimal model, at 0 eV the chemical potential intersects only the K pocket near the valence band maximum, while at −0.3 eV the chemical potential intersects the additional pocket at Γ. The density of states originating from the K pocket is expected to live in the center of the triangular sites, while the contributions from Γ live at the atomic sites and become more significant as the filling is lowered. The LDOS at these respective energies is shown in Fig. S1b,c, in which one indeed observes a shift from the charge living in the centers of the triangular lattice to the atomic sites.

In the main text, we explained this shift by describing the Bloch function as a linear combination of Wannier orbitals at the different sites. A complementary viewpoint is to consider the Bloch wavefunction as a linear combination of the original atomic d orbitals, rather than the valence band Wannier function. Near K, the Bloch wavefunction possesses $d_{xy} \pm i d_{x^2-y^2}$ character; this chiral orbital undergoes a phase winding around the atomic sites: note that the in-plane angular dependence of this chiral combination of the d orbitals takes the form $d_{xy} \pm i d_{x^2-y^2} \sim \cos 2\theta \pm i \sin 2\theta$. As shown in Fig. S2, the phases add destructively at the atomic sites, but add constructively in the centers of the triangles. Hence, the off-centered charge density arises simply as a result of the phase winding of the Bloch function at the VBM (as has been discussed previously in the case of quantum spin Hall insulator indenene [9, 44]). It is interesting to note that the chirality of the VBM has a range of important ramifications for the optical properties of TMDs [55]; our results highlight the manifestation of this orbital chirality in STM.

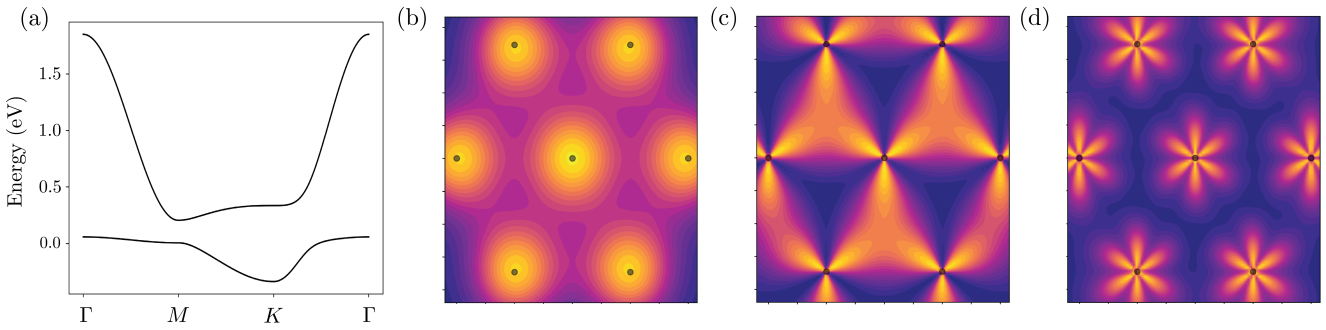

FIG. S3. **Simulated local density of states in the $s+f$ orbital model.** (a) band structure of the $s+f$ orbital model defined in Eq. (S12). The model exhibits no C_3-enforced topological obstruction, as the transformation of the orbital weight under C_3 is the same at Γ and K. (b) Near the Γ point where the orbitals are predominantly s character. (c) Near K, the band is an equally mixed $s+f$ orbital, which possesses a "fidget spinner" like profile which strongly overlaps with neighbouring orbitals in the center of the triangles. One might therefore expect that the LDOS is concentrated in the center of the triangles. (d) LDOS of the $s+f$ model for $E=-0.33$ eV, where the Fermi surface is near K. The combination of the fidget spinner orbital with the Bloch phase $e^{i\mathbf{K}\cdot\mathbf{R}}$ results in destructive interference between neighbouring orbitals, canceling out the large contribution to the density of states at the triangle centers.

B. Charge density in a two-band model of $s+f$ orbitals

In this section we further clarify the origin of this effect using a fine-tuned two-band model to highlight that the spatial profile of the wavefunction at a given point in momentum space does not on its own determine the maximum of the charge density. A "fidget spinner" type charge profile can be produced by an equal combination of an s-orbital with an f-orbital $s+f$ shown in Fig. S3c, possessing the angular dependence $\sim(1+\cos(3\theta))$. We construct a tight-binding model for which the valence band has pure s character near the Γ point, yet has $s+f$ character at the K point.

The model is given by

$$\mathcal{H}(\mathbf{k})=\begin{pmatrix} t_s(3+\gamma(\mathbf{k})) & t_p\gamma(\mathbf{k}) \\ t_p\gamma(\mathbf{k}) & t_f(3+\gamma(\mathbf{k}))\end{pmatrix} \tag{S12}$$

where $\gamma(\mathbf{k})=\cos(\mathbf{k}.\mathbf{a}_+)+\cos(\mathbf{k}.\mathbf{a}_-)+\cos(\mathbf{k}.(\mathbf{a}_++\mathbf{a}_-))$, and the 2×2 matrix acts on the space of (s,f) atomic orbitals; we shall choose $t_s=0.00655$ eV, $t_f=0.2055$ eV, $t_p=-0.0646$ eV in what follows.

The band structure is shown in Fig. S3a; the model is fine-tuned to produce pure s-orbital character near Γ and an exactly equal mix $s+f$ orbital character near K. Fig. S3c shows the real space profile of the $s+f$ orbital, showing maximal charge density at the centers of the triangles rather than on the atomic sites. Yet, the C_3 eigenvalue of the wavefunction at both Γ and K is trivial in this case, since both s and f orbitals are invariant under threefold rotations. Hence, the valence band in this model is not obstructed.

When we compute the local density of states at Γ, we find localised charge maxima on the atomic sites (Fig. S3b), as expected. Yet, when we compute the LDOS near K, we do *not* find a charge maximum living in the centers of the triangles. Rather, it is clear that the charge living in the center of the triangles has been eliminated by destructive interference, leaving only the portion of the $s+f$ orbital closest to the atomic site (Fig. S3d). Without a non trivial C_3 eigenvalue from the orbital weight, the Bloch phase $e^{i\mathbf{K}\cdot\mathbf{r}}$ results in destructive interference at the triangle centers; it is therefore necessary for the orbital character to transforms non trivially under C_3 in order for the charge to be located in the centers of the triangles.

This fact has already been discussed in theory work by Eck et al. [44], who observed that chiral $p_x\pm ip_y$ orbitals located on the $1a$ positions produce a charge maximum in the center of the triangles i.e. $2b$ positions, a result they use to explain the charge profile seen in STM imaging of indenene [9].

S2. ADDITIONAL DFT CALCULATIONS

Here, we present the band structure and partial charge density of hBN as a function of bias voltage. In Fig. S4a we plot the band structure of hBN around the Fermi level. The valence band is primarily composed of p_z-like states, as shown in the orbital decomposition. We calculate the partial charge density up to a voltage V_{bias}. Unlike the case of the obstructed atomic limit in WSe_2 (as shown in the main text), the charge density in hBN does not evolve with bias

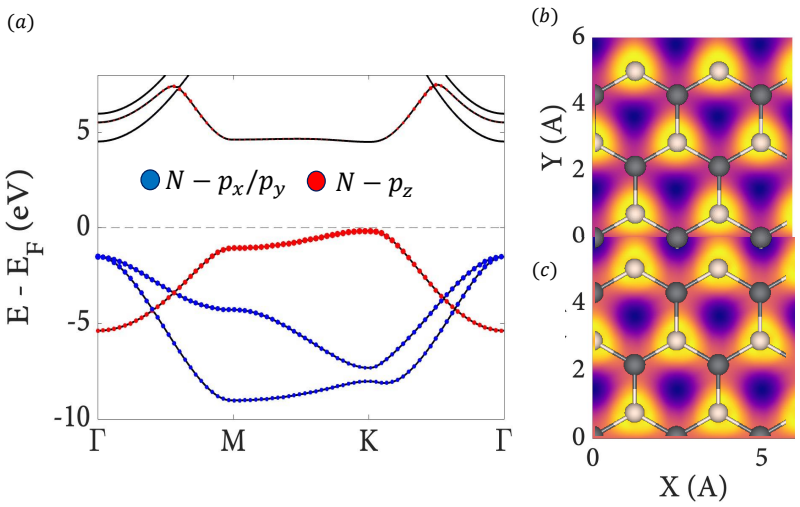

FIG. S4. **Band structure and charge density of hBN for two bias voltages.** (a) Band structure with orbital projections. The valence band is mainly composed of p_z orbitals, centered on the nitrogen sites. Both the p_z and p_x, p_y states which make up the valence manifold are extremely weakly hybridized, admitting maximally localized Wannier functions plotted in Fig. 2 Colored circles represent the weight of atomic-like orbitals for N. (b) Charge density of states with $V_{\text{bias}} = -0.5V$, in the vicinity of the K point. (c) Charge density at $V_{\text{bias}} = -1.5V$, covering bands near Γ. In both (b),(c), black and white atoms superimposed on the charge density denote boron and nitrogen, respectively.

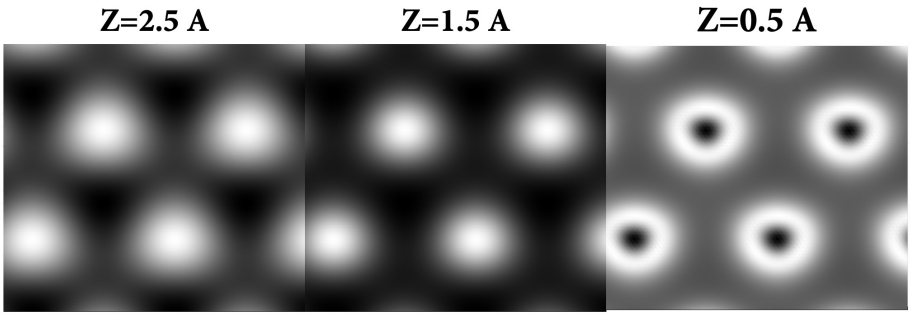

FIG. S5. **Varying the z component of the partial charge density in WSe_2.** The charge density in the vicinity of the Γ point is shown for three different heights. The bias is set to the same value as that in the main text.

voltage, as shown in Figs. S4b- S4c. As we vary the voltage following the procedure carried out in the main text – from states predominantly near K to those near Γ – the charge density does not exhibit any movement in real space. Orbital hybridization within the p manifold of N is much weaker than the corresponding d manifold in $WSe2_2$. The band composition of the band near Γ includes p_x, p_y orbitals, yet the states do not show any orbital interference due to the strongly localized nature of the wavefunction: the spread of the Wannier states $\sigma = 0.43a_0$, where $a_0 = 2.51$ Å is the lattice constant of hBN. This demonstrates the strength of our approach, allowing for distinguishing between trivial (hBN) vs non-trivial states (WSe_2).

A. Height dependence of simulated images

The shape of the charge density alone is insufficient to determine the topological properties. Below, we show that varying the tip height (the z projection of the partial charge density in simulation) changes the shape of the imaged states, without revealing additional information about a possible obstruction.

The distinct shape of the simulated charge centers shown in the main text and in Fig. S4(b)-(c) requires specification of the z projection of the partial charge density, $\rho(x, y, z)$. An immediate question is whether the tip position, reflected in z may evince any topological properties of the imaged charge. In Fig. S5, we vary the z projection from $2.5\mathring{A}$ to $0.5\mathring{A}$ in imaging the charge density of WSe_2. We find a gradual deformation of the orbital shape, until the annular pattern

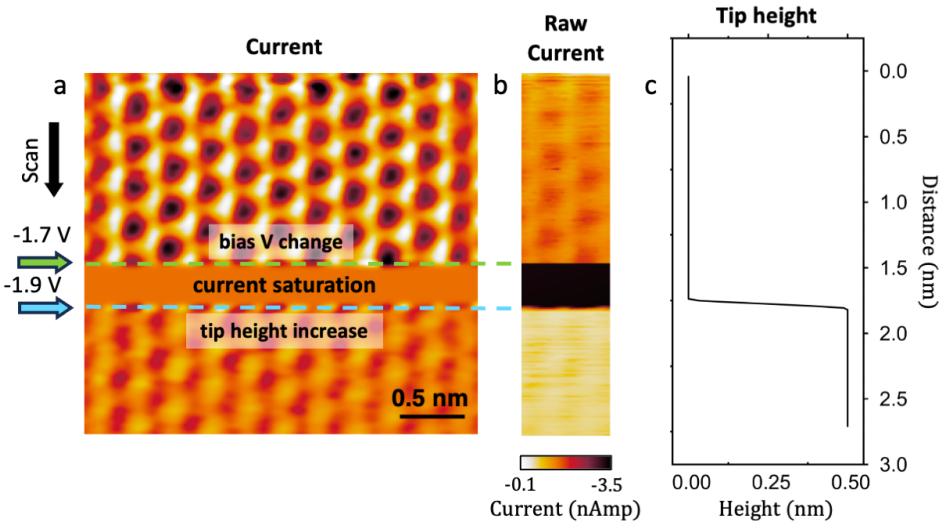

FIG. S6. **Detailed description of STM current imaging procedure** (a) STM current image at constant tip height. The scan begins at -1.7 V (top), then the bias was changed to -1.9 V (green arrow and dashed line), and the tip height was increased by 0.5 nm (blue arrow and dashed line). The image was flattened to lower the contrast and better visualize the different regions. (b) The corresponding raw current image showing the quantitative changes in the tunneling current amplitude (c) A height profile showing the tip position at the different regions of the current scan.

of the d-orbitals near Γ is apparent. While the charge seems to evolve with z height, it is clear that it is impossible to turn the topological nature of the states, even if an annular or off-atomic-site state appears when $z = 0.5\mathring{A}$. The precise determination of the topological properties requires probing the band at different energies, hence the unique advantage of our approach.

S3. EXPANDED DISCUSSION ON STM MEASUREMENTS OF WSe_2

Here we include additional technical discussion regarding our strategy to measure the energy dependence of the local density of states. One commonly used method is to perform dI/dV spectroscopy maps, where a full spectrum is obtained at each pixel. This enables comparison of the LDOS at different energies at the same spatial position. However, this procedure is typically performed by establishing constant current feedback at each pixel, resulting in a variation of tip-sample height between pixels. The contrast in such spectroscopic maps can arise from this feedback artifact, and is not a reliable indicator of shifts in the probability density in our case. Another typical technique is to obtain constant current topography measurements at the same location with different bias conditions. In this case, it is difficult to compare the spatial features in images obtained consecutively, as lateral drift can occur between images, especially at room temperature. While both techniques are conceptually simple, these complicating factors must be accounted for. For this reason we determine that topography and current measurements where the bias is changed mid-frame is the most reliable way to capture the energy dependence of the LDOS.

A. Supplemental description of the measurement procedure of the STM current image

In this section we outline the procedure for obtaining the current STM images included in Fig. 3f of the main text. Supplementary Fig. S6a shows an STM current image that begins at the top of the frame at a sample bias of -1.7 V with a constant tip-sample height (feedback disabled). As discussed in the main text, the tip must be closer to measure the tunneling current at this bias voltage because only states with a large tunneling decay constant near the K point are probed. When the sample bias is changed to -1.9 V (green dotted line) the states near the gamma point are also probed, and the current is saturated due to a sharp increase in tunneling. Supplementary Fig. S6a is a flattened current image that clearly shows the different bias regions, and Supplementary Fig. S6b shows the corresponding raw current image that quantitatively shows the order of magnitude increase in the tunneling current amplitude. To resolve the lattice, the tip was moved away from the surface by 0.5 nm (blue dashed line) to decrease the current, as indicated by the corresponding height profile in Supplementary Fig. S6c. The same procedure was followed to obtain

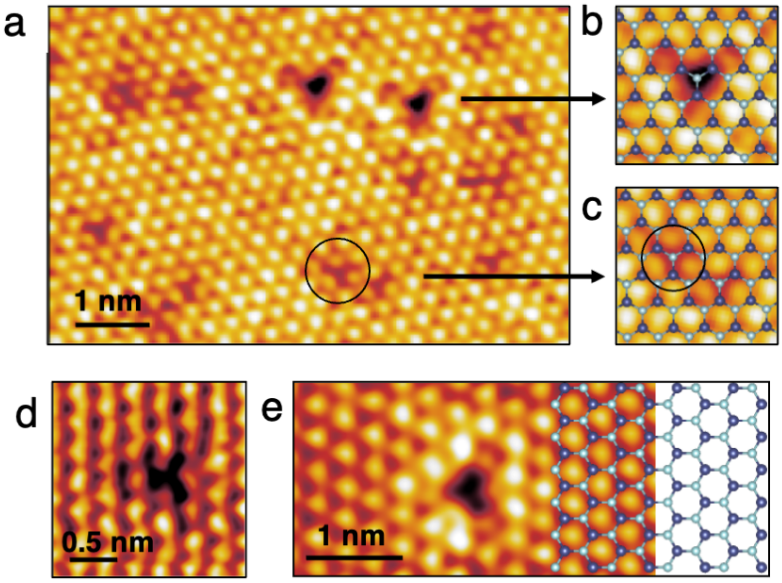

FIG. S7. **Analysis of the WSe_2 lattice alignment with the STM images** (a) STM image of the S doped WSe_2. (b) O substitutional impurity on an Se site. (c) S impurity on the Se site with a circle added to guide the eye. (d), (e) O impurities on the Se sites obtained near the STM images in Fig. 3 of the main text. The WSe_2 lattice overlay shows the alignment determined from the Se site impurity positions. The sample bias in (a,b,c,e) is -1.8 V and (d) is -1.6 V.

the current measurement in Fig. 3f of the main text, but the bias and tip height were adjusted simultaneously to produce a seamless image without current saturation.

B. Defect analysis to determine the WSe_2 atomic lattice alignment

Here we describe the method we used to determine the alignment of the WSe_2 atomic lattice in the STM images in Fig. 3 of the main text. Supplementary Fig. S7a shows an STM image of the S doped WSe_2, that shows the S dopants along with an additional defect type. These defects closely resemble the oxygen impurities substituting an Se site that were previously reported in $MoSe_2$ [20]. Supplementary Figs. S7b,c give a closer comparison of the two defect types. With the known lattice site of the S defects and knowing that STM probes the honeycomb center at a sample bias near the K point (as shown in Fig. 1 of the main text), we can accurately align the atomic lattice in the images. This analysis shows that the unknown defects are located at the Se sites, supporting the conclusion that they are O impurities on the Se sites. We will refer to them as Se site impurities. With this insight, we can use the Se site impurities to determine the lattice alignment of the STM images of the undoped WSe_2 monolayers in 3. Supporting Figs. S7d,e show images of the Se site impurities obtained at locations near the STM images in 3. From these images we determine the location of the Se sites and align the WSe_2 atomic lattice.